

See discussions, stats, and author profiles for this publication at: <https://www.researchgate.net/publication/335356314>

Fingertip Tactile Sensor with Single Sensing Element Based on FSR and PVDF

Article in IEEE Sensors Journal · August 2019

DOI: 10.1109/JSEN.2019.2936304

CITATIONS

0

READS

189

8 authors, including:



Ang ke
Huazhong University of Science and Technology

14 PUBLICATIONS 8 CITATIONS

[SEE PROFILE](#)



Jian Huang
Huazhong University of Science and Technology

224 PUBLICATIONS 2,262 CITATIONS

[SEE PROFILE](#)



Zhaolong Gao
Huazhong University of Science and Technology

9 PUBLICATIONS 85 CITATIONS

[SEE PROFILE](#)



Changyong Wang

8

78 PUBLICATIONS 1,642 CITATIONS

[SEE PROFILE](#)

Some of the authors of this publication are also working on these related projects:



Decode stand/squat with cortical neuronal spikes [View project](#)



[Neural Rehabilitation](#) [View project](#)

Fingertip Tactile Sensor with Single Sensing Element Based on FSR and PVDF

Ang Ke, Jian Huang, *Senior Member, IEEE*, Luyao Chen, Zhaolong Gao, Jiuqi Han, Changyong Wang, Jin Zhou, and Jiping He, *Senior Member, IEEE*

Abstract—The fingertip sensor is essential for the closed loop control of prosthetic hand, while the development of a tactile sensor with a balance in the cost and performance is still a challenge. This paper presents the development of an anthropomorphic fingertip sensor for prosthetic hands. The structure of our sensor mainly consists of a force sensing resistor (FSR) sensor module and a polyvinylidene fluoride (PVDF) sensor module. The PVDF sensor module is made up of a circular truncated cone shaped PVDF film that wrapped in a polydimethylsiloxane (PDMS) substrate. The PVDF sensor module plays two roles in the tactile sensing task. First, the dynamic low frequency response of the PVDF is used for dynamic contact point estimation. Second, the high frequency response of the PVDF is used for texture recognition. An FSR sensor module is used for static force measuring. Experimental results show that the sensor has a good performance in contact force measuring, contact point estimation, and texture recognition. The force measurement error of normal force is less than 5% at the most sensitive subareas, and the sensor is capable of distinguishing five subareas of the sensitive part at an accuracy over 96%. It also can recognize five different textures with an accuracy of $94.1\% \pm 0.7\%$.

Index Terms—Fingertip Sensor, Tactile Sensor, Contact Location, Texture Discrimination.

I. INTRODUCTION

TACTILE sensing is essential for autonomous manipulation and grasping control of the prosthetic hands [1]. Besides the application of prosthesis, tactile sensing is also an essential element for dexterous robot hands and manipulators that have the requirement of autonomous manipulation [2]. A tactile sensor provides information about interaction force and surface properties at the contact point [3]. In prosthetic hand applications, the required tactile sensing information for autonomous manipulation and haptic feedback includes the contact force and the surface properties such as texture and hardness [2].

It still remains a challenge for the development of a functional and low-cost tactile sensor that can be used in prosthetic hands, since there are many constraints that should

This research was supported by the Research Fund of PLA of China (BWS17J024), the Fundamental Research Funds for the Central Universities (HUST: 2019kfyRCPY, 2019kfyXKJC019) and the National Natural Science Foundation of China (61233015 and 61473130).

A. Ke, J. Huang, L. Chen, and Z. Gao are with Key Laboratory of Ministry of Education for Image Processing and Intelligent Control, School of Artificial Intelligence and Automation, Huazhong University of Science and Technology. (*Corresponding author: J. Huang.*)

J. He is with Beijing Advanced Innovation Center for Intelligent Robots and Systems, Beijing Institute of Technology.

J. Zhou and C. Wang are with Department of Neural Engineering and Biological Interdisciplinary Studies, Institute of Military Cognition and Brain Sciences, Academy of Military Medical Sciences.

be considered. In [2], Zhanat summarized some criteria with the guidance for tactile sensors design in robot hand applications, such as high spatial resolution, high sensitivity, broad frequency response, low hysteresis and memory effect, robust in performance, and so on. In the practical design, some of these criteria may be contradictory to each other. For instance, a higher spatial resolution may inevitably leads to vast wire connections, and too many wire connections may lead to a stronger sensitivity to noises. Besides the functional performance, the design of a tactile sensor should also consider the trade-off between the performance and the cost [3]. Many commercial prosthetic hands are dexterous in movement but still lack of tactile sensing for interactions, such as the i-Limb hand [4], the Bebionic hand [5], the VINCENT hand [6], and so on. One of the most important reasons is that the high cost of tactile sensor hinders its wide applications.

So far, the force measuring of tactile sensor can be achieved by many methods, such as piezoresistive effect [7], piezoelectric effect [8], quantum tunnel effect [9], optical tactile transducer that based on nanocomposite material [10], pneumatic feedback actuators [11], or even sophisticated design that based on optical fibers [12], [13]. The commercially available FSR is a kind of widely used piezoresistive sensors [14]. In [2], Zhanat provided a detailed review about force measuring in tactile sensing. However, in order to achieve contact point estimation, almost all methods adopt a high spatial resolution tactile sensing array (see the works introduced in [7]–[9], [15]–[20]). In a tactile sensing array, every sensing element is responsible for single-point force measurement, an array of sensing element is arranged to form a large sensitive area. The contact force strength and contact point can be inferred from the matrix output of all sensing elements. In [18], Yu proposed a flexible tactile sensor array based on the PVDF, which consists of a 3×2 sensor unit matrix. Each unit includes four upper electrodes, one lower electrode and the PVDF film is sandwiched between electrodes. In [17], [21], Alexander introduced the design of an integrated fingertip tactile sensor for the humanoid robot iCub. The capacitive pressure sensor system is made of flexible PCBs that has 12 sensitive zones and shaped approximately like a human fingertip. In [7], Risto introduced a way to produce 3D-shaped tactile sensors with laser structuring technology. The flexible conductive piezoresistive rubbers and a non-flexible pattern of electrodes form a two-layer structure. In this way, they developed a tactile fingertip sensor that incorporates 12 tactile elements for the Shadow Robot Hand. There are also many commercial planar array sensors suitable for robot hands, such

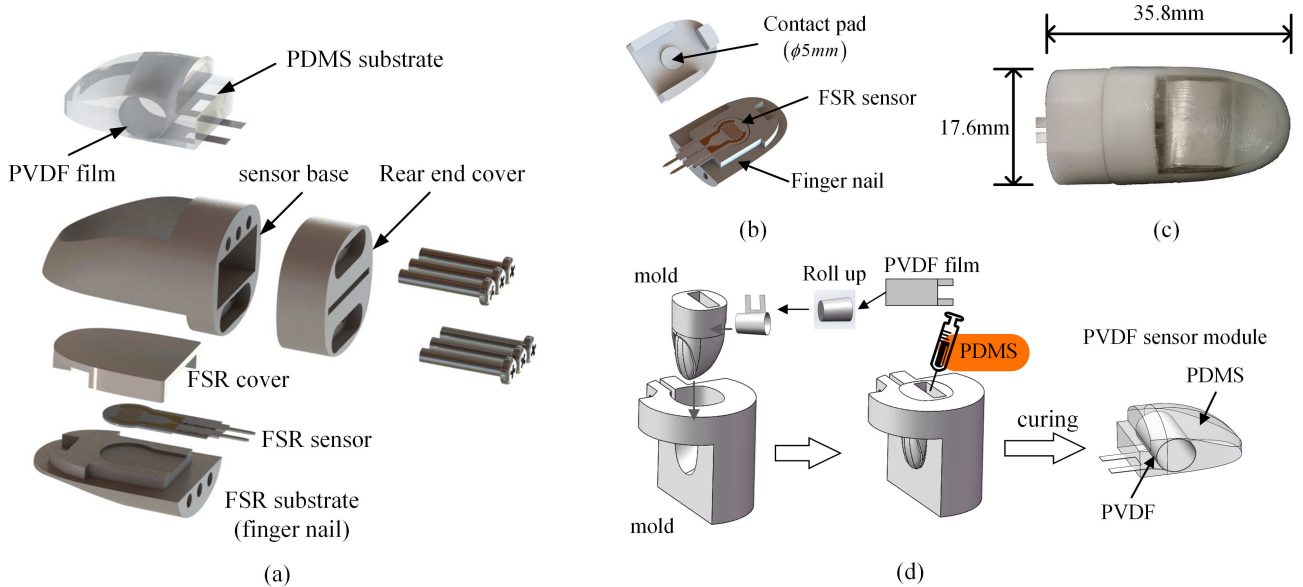


Fig. 1. (a) The overall structure of modular fingertip sensors, which has an anthropomorphic appearance. It consists of three main components: the FSR sensor module, the PVDF sensor module, and the supporting and protection substrate structure. (b) The detailed structure of the FSR sensor module, in which the contact pad is used for improving the sensitivity and stability of FSR sensor. (c) The well-fabricated fingertip sensor and its main dimensions. (d) The fabrication procedure of the PVDF sensor module.

as the matrix pressure mapping sensors from Tekscan [22], the finger tactile pressure sensing system from Pressure profile Systems [23], the WTS-FT tactile sensing module from Weiss Robotics [24], the BioTac tactile sensor from SynTouch [25] and so on.

Although tactile sensing array have excellent performance in spatial resolution, they are also strongly dependent on special processing equipment, such as the Micro-Electro-Mechanical System (MEMS) technology [19], electrospinning [26], screen printing [20], laser structuring [7], and so on. Furthermore, due to a large number of sensor elements that used, the processing circuit may be large and complex, which leads to the high cost and price of products.

Texture information of local surface is also an important element in autonomous manipulation and human robot interaction [2]. In most case, texture recognition is based on vibration measurement [27]. The piezoelectric sensor such as PVDF is an ideal material for texture recognition, it has many excellent characteristics, such as ultra-sensitivity, high deformability, wide frequency response, and low permittivity [26]. Many studies about PVDF films just focus on the high frequency response for texture recognition, while few of them utilize the PVDF for low frequency motion monitoring. However, the low frequency response information of PVDF sensors can also be useful in some cases, e.g. in [28], the PVDF nano fiber is used for human motion monitoring. A data glove that based on PVDF nano fiber sensors can accurately monitor the finger motion with frequency of about 1 Hz.

In this works, we show that when combining the nonuniform deformation and the high sensitivity of PVDF film, the dynamic low frequency response of PVDF can be used for dynamic contact point estimation, while the high frequency response can be used for texture recognition. To achieve the

static force measuring, an FSR is adopted as a complementary. Thus, we can achieve normal force measuring, contact point estimation, and texture recognition via only one sensor element, without using complex sensing array. The design combines the advantages of the PVDF for dynamic contact force measuring and the convenience of FSR in static force measuring. Compared with other designs that also combine the PVDF and FSR in tactile sensor, this work puts forward a novel design. Thin film PVDF is rolled into a circular truncated cone shape and then buried into the elastic material PDMS. An FSR (FSR 402, Interlink Electronics, Inc., Los Angeles, CA, USA) placed under the PVDF sensor module is used for static force measuring. The whole structure of the fingertip sensor is very compact with a modular design, the finger-shaped sensor can be directly used as the distal phalanges of the prosthetic hands. Compared with traditional tactile sensor solutions, the contribution of this work are mainly in two aspects: First, our proposed method gives a pilot study that using a single sensing element for contact point estimation, which involves the utilization of the low frequency response of PVDF. Second, we proposed a novel, compact and low-cost design of a fingertip tactile sensor with commercially available PVDF and FSR. The proposed sensor has satisfactory performance in force measuring, contact point estimation and texture recognition.

The organization of this paper is introduced as follows. First, in section 2 we introduce the detailed structure of the fingertip sensor, and a brief analysis of the operating principle is also illustrated. Section 3 describes the experimental setup and the experimental procedure to evaluate the performance of the sensor. Then the data analysis method is put forward in section 4. Section 5 shows the detailed results of each experiment. In section 6, a discussion about the result is given. Finally, a

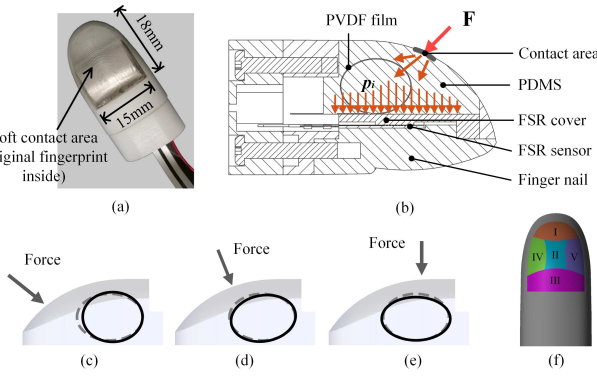


Fig. 2. (a) The appearance of the fabricated sensor and the dimension of its sensitive part. (b) An illustration of the principle analysis, due to the elasticity of PDMS, the contact force transited from contact area to the FSR cover and PDMS is non-uniform and asymmetric. (c-e) An example of the deformation of PVDF under different contact force. (f) A partition of the sensitive surface, the whole sensitive surface is roughly divided into five subareas.

conclusion about this work is given in section 7.

II. STRUCTURE AND PRINCIPLE ANALYSIS

A. Design of the integrative fingertip

The whole mechanical structure of the modular fingertip sensor is shown in Fig. 1(a). The fingertip sensor includes three main components: the sensor base, the PVDF sensor module, and the FSR sensor module. A rear end cover is used for electrical protection and mechanical support. The whole proposed sensor module is very compact and can be directly integrated into the prosthetic hand design. The structure of the main body, fingernail and rear end cover are printed directly by the stereo lithography appearance (SLA). Note that the SLA technology is more detailed and precise than the fused deposition modeling (FDM).

The FSR sensor module has a sandwich structure, i.e. a small FSR (Interlink, IE402) is sandwiched between the cover and substrate. To improve the sensitivity and uniformity of FSR, a hard flat contact pad that matches the sensitive area of FSR is used. The diameter of the contact pad is 5mm, matching the most sensitive area of FSR, as shown in Fig. 1(b).

The PVDF sensing component is fabricated by casting. First, we made two moulds that match the shape of fingertip pad. Then a PVDF film was curved into a circular truncated cone shape and was placed into the cavity. Finally, we filled the hole with PDMS. After a curing procedure in 60 degrees Celsius which lasted for about 24 hours, we took out the PVDF sensor packaged by PDMS. This procedure is shown in Fig. 1(d). The final dimension of the fabricated sensor is about 17.6mm x 16.4mm x 35.8mm (including the rear end cover for handling).

B. Working analysis of the sensor

In this subsection, we present the working principle of the structure of our design. As shown in Fig. 2, when the finger contacts an object and is acted on by an external force at different subareas of the sensitive area, due to the

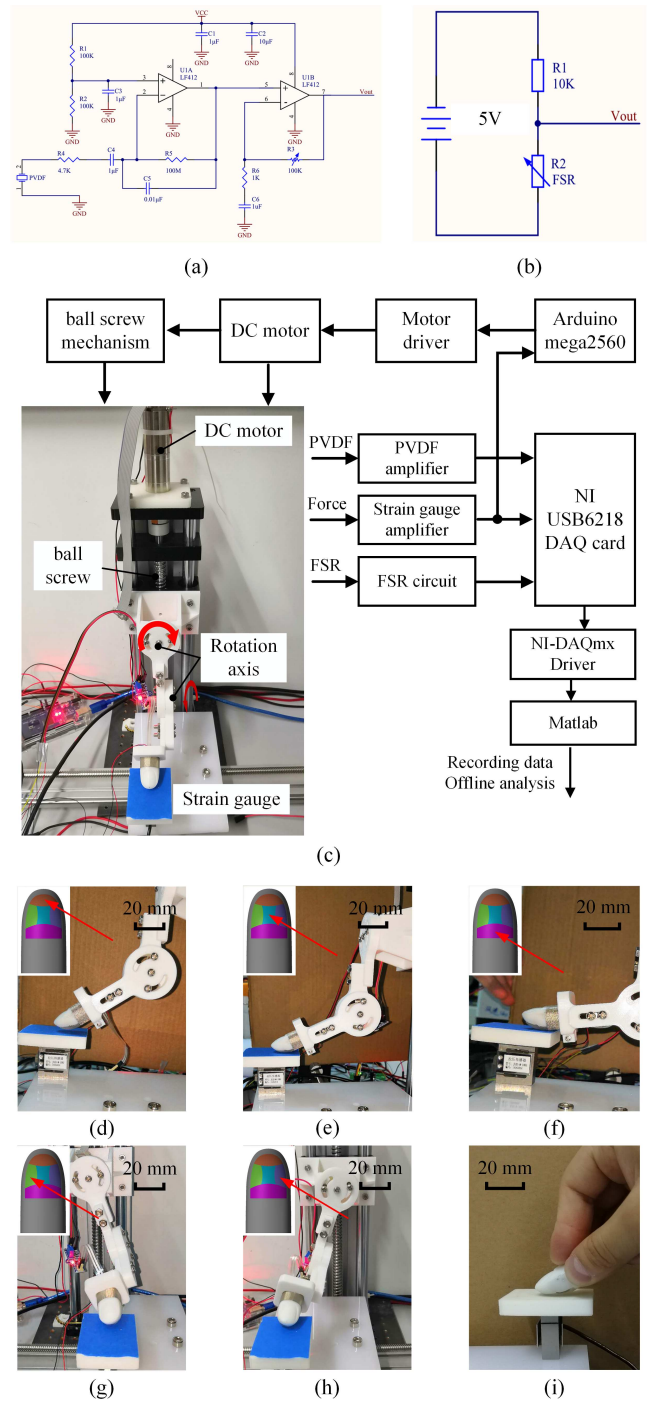


Fig. 4. (a) Part of the main schematic diagram of the PVDF. The primary circuit consists of a charge amplifier and an operational amplifier. (b) Measurement circuit of the FSR, in which the resistance of referent resistor R1 is 10K Ω . (c) An overview of the experimental setup and data flow, the loading system is a home-made ball screw table that controlled by an Arduino board. (d)-(h) Five postures of the clamp during the experiment. (i) The sensor is loaded by the hand of the operator.

deformation of PMDS substrate, the transition of pressure in the PDMS substrate is non-uniform, as well as the deformation of the PDMS block. On one hand, this results in a different deformation of the PVDF film, as illustrated in Fig. 2(c-e). Since the PVDF is highly sensitive to strain, little different contact force will result in a sizeable different response of the PVDF. This characteristic may give the sensor the potential to distinguish the contact point location. On the other hand, because of the nonuniform deformation of the PDMS, the pressure distribution on the FSR cover also changes according to the contact point, as shown in Fig. 2(b). This phenomenon along with the PVDF may also give the sensor the potential to distinguish the contact point location. Since the contact point location will also influence the response of FSR, in order to reduce the error of force measurement, the model used to calibrate the FSR should take the term of contact point location into consideration if this influence becomes non-ignorable.

Fig. 3 gives an illustration of the behaviour of our fingertip sensor during working. Fig. 3 (a) shows a typical situation that a finger equipped with the fingertip sensor approaches an object. Fig. 3 (b) and Fig. 3 (c) show the response of the FSR and the PVDF when the contact force increases from zero to dozens of Newton during the grasping process. According to the response of the FSR and the PVDF at different contact force and different contact area, the working principle of the sensor can be explained as below:

- When the contact force is relatively small, owing to the buffer of the elastic PDMS, the response of the FSR is little influenced by the contact area, as illustrated in Fig. 3 (b). However, due to the high sensitivity of the PVDF and our structure design, the location of the contact point has a significant influence on the output signal of the PVDF, even though the contact force is small. Since the PVDF has a very wide frequency response, in this stage, the low frequency response of the PVDF caused by the different location of the contact point can be used to estimate the location of the contact point.

- When the contact force continues to increase, the influence of contact point location on the response of FSR emerges. To get a more precise measurement of force, we need to take the location of the contact point into consideration during force prediction. The required information about the location of the contact point can be inferred during the stage when the contact force is small, as explained above.

According to the above analysis, if we combine the information of the FSR and the PVDF, the sensor is capable of both force measuring and contact point estimation. We also found that when using the 3D printed mould based on the FMA technology (layer by layer printing) for PDMS casting, the surface of the PDMS has an original fingerprint, without needing any other further special handling (see in Fig. 2(a)). The fingerprint is an essential structure of the human fingers; it has been widely proved that the fingerprint can increase the friction during grasp and can also improve the perception of texture.

III. EVALUATION OF SENSOR PERFORMANCE

A. Experimental setup

During the experiments, a strain gauge force sensor and its corresponding amplifier for force measuring are used for calibration. We also developed a custom platform driven by a DC motor (Maxonmotor Inc.) for loading. It contains a two-degree-of-freedom clamp, which can be used to hold the sensor in different orientation. An Arduino Mega2560 board is used as the controller. The controller collects the value of strain gauge in real time, then it sends commands to the driven board to control the motion of DC motor. The whole loading system is shown in Fig. 4(c). An analogue-to-digital converter NI USB-6218 (National Instruments) is used for data collecting. As shown in Fig. 4(a), the main component of the PVDF amplifier is a dual-input operational amplifier LF412 (Texas Instruments). The output of PVDF is the electrical charge.

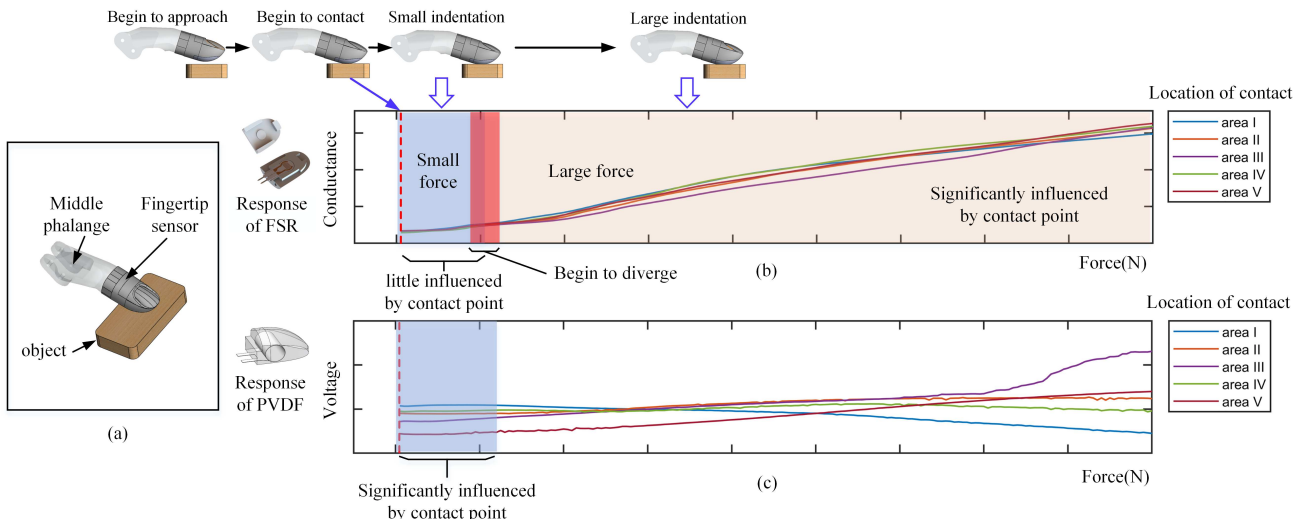


Fig. 3. (a) An illustration of a finger equipped with fingertip sensor begins to approach the object. (b) The response of FSR during the grasp process. (c) The response of PVDF during the grasp process.

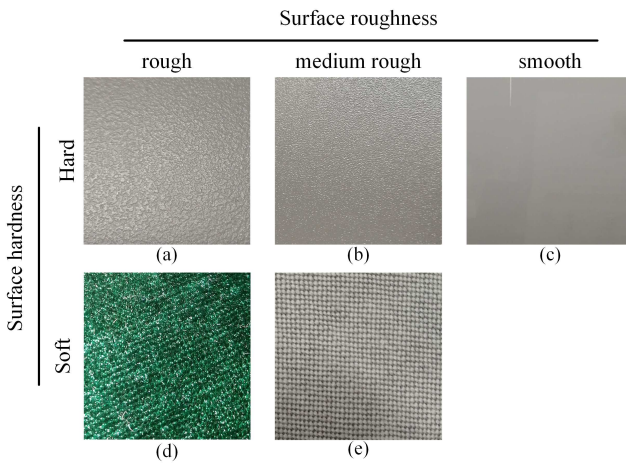


Fig. 5. Five textures of different materials that used in experiment II for texture recognition. (a) Table surface. (b) Frosted plastic sheet. (c) Acrylic sheet. (d) Flannelette. (e) Cotton cloth.

First, we need to convert the change of charges into the change of voltage, then amplify this voltage for further analogue-to-digital converting. The FSR is a kind of piezoresistive element. The resistance value of FSR can reach several million Ohm when no force applied, and they may drop to several kilo Ohm when there is a force acted on it. The classical measuring circuit to capture the change in resistance is a voltage divider, as shown in Fig. 4(b), in which the value of the reference resistance R_1 is $10\text{ K}\Omega$. As shown in Fig. 4(c), the output of strain gauge is first conditioned and amplified, then connected to the NI USB-6218 for analogue-to-digital converting. The signals of the FSR, the strain gauge and the PVDF are all digitalized at a frequency of 1000Hz. For the convenience of data analysis, digital signal recording procedure is performed in Matlab (MathWorks Inc.) with the software support of NI.

B. Evaluation experiment

To get a comprehensive evaluation of the performance of the fingertip sensor, we conduct two experiments. First, periodic loading experiment to study the robustness of force measuring and the feasibility of the sensor to estimate the contact area by the low frequency response of the PVDF. Second, we conduct an experiment to evaluate the ability of texture recognition of our fingertip sensor. Texture recognition is a beneficial function for prosthetic hands because users have strong desire to perceive the texture that they touched by prostheses, and this may be achieved by combining the sensing results with the brain-machine interface technologies. The detailed procedures and details about each experiment are introduced in the following.

1) *Experiment I*: First, the sensor is fixed on the clamp. The orientation of the finger is adjusted by the two-degree-of-freedom clamp, so that we can change the contact location for normal loading. The force range of periodic loading is set to be between 0 and 20N, which is controlled by the Arduino board according to the force feedback to it. The loading system is run at a uniform speed about 1mm/s. For each subarea illustrated in Fig. 2(f), we adjusted the clamp to make the

loading force direction perpendicular to the contact surface, the five postures are shown in Fig. 4(d)-(h). The loading procedure for each subarea was repeated 180 times. The collected data are used for the robustness analysis of FSR, force calibration of FSR, and also contact point estimation. For the contact point estimation, the total data sets (including training set and testing set) have 900 samples.

In practice, the contact position of fingertip sensor is hard to be kept the same as the loading device can do, therefore we need an evaluation that is closer to practical application. That is, for each subarea, we let the contact position and the pressing direction both fluctuant in a small ranges. To realize this, the sensor is held by the operator to be pressed on the top platform of strain gauge sensor with an approximately uniform speed, as shown in Fig. 4(i). For each subarea, we repeat for 50 times.

2) *Experiment II*: Five typical textures in daily life are chosen for texture recognition experiment, representing different hardness and roughness. The pictures of these five textures are shown in Fig. 5. The primary physical features are annotated above each figure. During the experiment, the finger sensor is held by the operator to slip on different surfaces with a suitable pressure force ($3.20 \pm 0.57\text{N}$, $2.44 \pm 0.32\text{N}$, $3.53 \pm 0.68\text{N}$, $3.16 \pm 0.32\text{N}$ and $3.91 \pm 0.39\text{N}$, from subarea I to IV respectively), the detailed statistic information after experiment is shown in Table I. The contact region is the central part of finger bed (subarea II). Other factors such as slip speed are roughly controlled by the operator.

IV. DATA ANALYSIS METHODS

A. Pretreating of data

In this work, the contact force is measured by the strain gauge. The original signal of the strain gauge must be converted into actual force value, which can be realized by a pre-calibration procedure with standard weights. The strain gauge shows a very ideal linear relationship to pressure (RMSE = $7.744\text{e-}05$). Therefore the actual force can be easily calculated from the output voltage of the strain gauge. The raw signal of FSR sensor is transformed into the conductance value according to the parameters of the measurement circuit:

$$\frac{R_{fsr}}{R_1} = \frac{V_{CC} - V_{out}}{V_{out}}, \quad (1)$$

$$C_{fsr} = \frac{1}{R_{fsr}} = \frac{V_{out}}{V_{CC} - V_{out}} \cdot \frac{1}{R_1}, \quad (2)$$

where V_{out} is the measured voltage across the reference resistor, while R_1 is the value of reference resistor. In this work, we choose a $10\text{K}\Omega(\pm 1\%)$ resistor as the reference resistor.

A sliding smooth procedure with a time window of 50ms was then applied to both the conductance value and the actual force value to remove the sharp corner. The raw PVDF signal is filtered by an IIR notch filter ($Q=35$) to remove the power-line interference of 50Hz tone. To avoid the lag in signal phase, all the filtering procedures are performed by zero-phase filtering technology. For each test, we have obtained statistics about the maximum loading force during experiment I. The results are shown in Table I.

B. Analysis of the robustness of FSR module

The robustness of sensor means that the response of sensor should withstand high repeatability in different measurement. In this work, according to the analysis in section II, we need to test whether the response of FSR has consistency in the same subarea. Meanwhile, we also need to have an evaluation about the difference of FSR response if the contact point locates in different subarea.

If the response of FSR sensor during different experiments at the same contact area has a consistency, we can say that measurement from the same area obey the normal distribution. The problem is then reduced to the distribution test. Here we need to test the following two hypotheses:

H0: The distribution of measured conductance corresponding to the same force during independently repeated measurement is a normal distribution.

H1: The distribution of measured conductance corresponding to the same force during independently repeated measurement is not a normal distribution.

There are many methods used for normal distribution test, such as the Chi-square test, Anderson-Darling test, Lilliefors test, Kolmogorov-Smirnov test (K-S test) and so on [29]. In this work, we chose the Kolmogorov-Smirnov method. The Kolmogorov-Smirnov test method compares the difference between the cumulative distribution function (CDF) of the observation sample and the CDF of the reference distribution; if the difference between the two CDFs is small enough, it can be inferred that the sample is taken from a specific distribution family.

It is impossible to examine every continuous force value for distribution test. To simplify the problem, we examine a serial of discrete forces. Here we choose the force range from 0.1N to 20N with a step of 0.1N, totally resulting in 200 points of force. We denote them as f_i ($i = 1, 2, \dots, 200$). In each test, we first pick up the measured force point that is closest to each f_i during the pressing and releasing phases, and then record the corresponding conductance of FSR. This procedure is repeated for each discrete force f_i and each subarea. Thus for each subarea A_j ($j = 1, 2, \dots, 5$) and each force f_i , we finally get 100 samples (in experiment I, the loading procedure for each subarea was repeated 180 times,

and we choose the first 100 samples for each subarea), denoted as $u_{ij} := C_{P_k}$ ($k = 1, 2, \dots, 100$) for the pressing phase and $v_{ij} := C_{R_k}$ ($k = 1, 2, \dots, 100$) for the releasing phase. The Kolmogorov-Smirnov test is then performed in sample u_{ij} and v_{ij} respectively, the significant level is 0.05.

C. Calibration of FSR for force measuring

For a rough measurement, the conductance of FSR is considered to be a polynomial function with respect to the normal pressure [30], [31], or some other complex nonlinear functions [32]. However, there is non-negligible hysteresis for force measurement by using the FSR. There are many studies on the calibration of FSR, most of which focused on the compensation of hysteresis of FSR [33]–[35]. There are mainly two approaches to model the hysteresis of FSR. Some researches attempted to model the piezoresistive response of conductive polymer composites exactly by physical approaches [34], which can be very complex and still have large error during practical applications. Another method attempted to find a mathematic model that matches the measured data [36]. In our design, the hysteresis of the FSR in force measuring comes from two aspects, i.e. the hysteresis of PDMS substrate and the hysteresis of the FSR itself. Thus it is too difficult to find an accurate physical model for the compensation of the hysteresis of the FSR in force measuring. Here we adopt the calibration method put forward by Rick [36], in which the loading history was considered in the equation for calibration. The difference is that we use the conductance instead of the resistance for calibration, and the calibration equation is given by:

$$F_t = g(C_t) = a_0 + a_1 C_t + a_2 C_t^2 + a_3 C_t^3 + a_4 C_t^4 + b_1 I_t + b_2 I_t^2 + b_3 I_t^3 + b_4 I_t^4 \quad (3)$$

where C_t means the conductance of FSR at time t . F_t is the predicted force at that time t . I_t is the moving integral of the history output of C_t , and the integral interval of I_t is the sum of the measured conductance values obtained in the last 0.5s that multiplied by a linear increasing factor [36].

TABLE I
AN OVERVIEW OF THE DATA INFORMATION IN EXPERIMENT I AND EXPERIMENT II.

| contact point location | maximum pressure force for each test | | | | | Test times | |
|------------------------|--------------------------------------|------------|---------|----------|----------|------------|-----|
| | min (N) | median (N) | max (N) | mean (N) | s.d. (N) | | |
| experiment I | subarea 1 | 19.89 | 20.00 | 20.10 | 20.00 | 0.037 | 180 |
| | subarea 2 | 19.84 | 20.00 | 20.08 | 19.99 | 0.034 | 180 |
| | subarea 3 | 19.84 | 19.99 | 20.07 | 19.99 | 0.037 | 180 |
| | subarea 4 | 19.87 | 20.00 | 20.11 | 19.99 | 0.033 | 180 |
| | subarea 5 | 19.87 | 19.99 | 20.07 | 19.99 | 0.034 | 180 |
| experiment II | subarea 1 | 1.64 | 3.18 | 4.64 | 3.20 | 0.57 | 150 |
| | subarea 2 | 1.62 | 2.42 | 3.47 | 2.44 | 0.32 | 150 |
| | subarea 3 | 2.23 | 3.40 | 5.79 | 3.53 | 0.68 | 150 |
| | subarea 4 | 2.34 | 3.18 | 4.13 | 3.16 | 0.32 | 150 |
| | subarea 5 | 2.75 | 3.96 | 4.84 | 3.91 | 0.39 | 150 |

D. Pattern recognition method for contact point location and texture discrimination

1) Feature extraction: Feature extraction is a crucial procedure before the classification task. It finds a robust representation of the characteristic of the original signal. In this work, for the classification of contact area and texture, we extracted several features for comparing. Here we give a brief introduction to the methods that are used to extract the feature vector from the original signal. The original signal recorded from the PVDF at i_{th} test is denoted as $\{X_i\} := x_{i_0}, x_{i_1}, \dots, x_{i_{M-1}}$, where M is the number of points in X_i .

(a) Wavelet Packet Decomposition (WPD)

The wavelet analysis is a powerful tool that provides a method to decompose an original signal into different scales and frequency bands for analysis. In this work, the original signal X_i is first decomposed into a tree over 6 levels by the Daubechies wavelet. Note that there are two nomenclatures in use for Daubechies wavelet. One of them is referring to the number of vanishing moments, denoted by dbN , where N is the number of vanishing moments. In this work, we adopt 3 types of wavelet, namely $db1$, $db2$, and $db3$, and the detailed definition and procedure can be found in [37]. The wavelet packet node energy at each root node is calculated to form the feature vector F_i :

$$E_k(W) = \sum_{j=1}^M (w_j^k)^2 \quad (k = 1, 2, \dots, 2^6), \quad (4)$$

and the feature vector is defined as:

$$F_i := [E_1, E_2, \dots, E_{64}], \quad (5)$$

where w_j^k is the j_{th} wavelet packet coefficient at k_{th} wavelet packet root node. M is the number of element at k_{th} wavelet packet node.

(b) Frequency Component (Freq. Comp.)

According to the Fourier transform theory, a temporal signal can be represented in the frequency domain by the Fourier transform. First, we apply a 512-point Fourier transform to the original signal X_i . The obtained result Y_i is a vector containing 512 complex numbers that represent the frequency components of the original signal. Then we select the real parts and imaginary parts of the first 12 elements of Y_i to form the feature vector F_i . The formula for the discrete Fourier transform of N points is given by [38]:

$$Y_{i_k} = \sum_{n=0}^{N-1} x_{i_n} e^{\frac{2\pi i}{N} kn} \quad (k = 0, 1, 2, \dots, N-1), \quad (6)$$

and the feature vector is defined as:

$$F_i := [real(Y_{i_1}), img(Y_{i_1}), \dots, real(Y_{i_{12}}), img(Y_{i_{12}})], \quad (7)$$

where $real(Y_{i_k})$ and $img(Y_{i_k})$ represent the real part and imaginary part of complex Y_i respectively.

(c) Frequency Amplitude (Freq. Amp.)

This method is similar to that proposed above. First, we apply a 512-point Discrete Fourier Transform (DFT) to the original signal X_i to represent the signal in frequency domain.

Then we calculate the amplitude at each sampling frequency to form the feature vector F_i :

$$F_i := [|Y_{i_0}|, |Y_{i_1}|, \dots, |Y_{i_{N-1}}|], \quad (8)$$

where Y_{i_k} ($k = 0, 1, \dots, N-1$) comes from Eq. (6).

(d) Power Spectral Density (PSD)

The Power Spectral Density (PSD) represents the strength of the energy as a function of frequency. It shows how the power of the signal is distributed over the frequencies. A simple method for estimating the nonparametric PSD is based on the result of DFT directly [38]. For an N -point DFT of original signal X_i , the periodogram estimate of the power spectrum of X_i is defined at $N/2 + 1$ frequencies as:

$$PSD_i(0) = \frac{1}{N^2} |Y_{i_0}|^2, \quad (9)$$

for $k = 1, 2, \dots, N/2 - 1$:

$$PSD_i(k) = \frac{1}{N^2} (|Y_{i_k}|^2 + |Y_{i_{N-k}}|^2), \quad (10)$$

for $k = N/2$:

$$PSD_i(N/2) = \frac{1}{N^2} |Y_{i_{N/2}}|^2, \quad (11)$$

and the feature vector is defined as:

$$F_i := [PSD_i(0), PSD_i(1), \dots, PSD_i(N/2)]. \quad (12)$$

(e) Autoregression Model (AR(p))

The autoregressive model specifies that the current output value of a system depends linearly on its previous output values and a stochastic term. The general form of an autoregressive of order p is defined as:

$$X_i(j) = a_0 + \sum_{k=0}^p a_k X_i(j-k) + \varepsilon_j, \quad (13)$$

where a_1, a_2, \dots, a_p are the parameters of the AR(p) model. a_0 is a constant and ε_j is the white noise. In this work we use an autoregressive model of order 2. The feature vector is formed by the parameters of the model AR(2):

$$F_i := [a_0, a_1, a_2]. \quad (14)$$

2) Classifier: The original signal of each sample is first descended dimension by the feature extraction method, this result in a feature vector that has the same dimension of each sample. Then, the data set that consist of the feature vectors and its corresponding labels are put into the classifier for pattern recognition. In this work, since we do not focus on the design of the best classifier, several common classifiers are chosen to evaluate the performance of our finger sensor. The classifiers we used include the k-Nearest Neighbor (kNN), the Support Vector Machine (SVM), the Discriminant Analysis (DA), and the Decision Tree (DT). There are many choices of super parameters and concrete structure for each kind of classifier, here we specified some commonly used parameter that also used by other researchers. For the kNN method, the value of k is set to be 1, 5 and 10. For the SVM method, the option of the kernel is set to be linear, cubic, radial basis function (RBF) and Gaussian function. While for discriminant

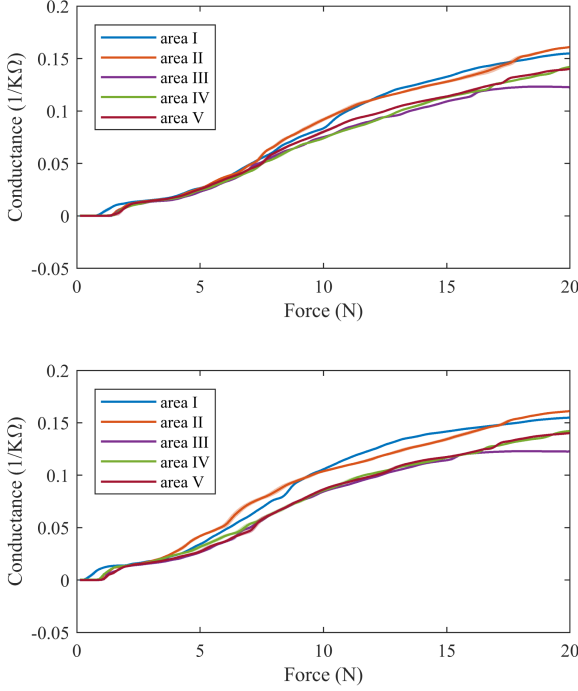


Fig. 6. The average relationship (mean \pm std.) between the pressure force and the conductance of FSR at the different contact area and different phase of loading respectively. (a) The pressing phase. (b) The releasing phase.

analysis, we use both the Linear Discriminant Analysis (LDA) and the Quadratic Discriminant Analysis (QDA). For the DT, the maximum split level is specified as 4, the corresponding classifier in our results is denoted by DT(4). For each classifier, we use the 5-fold cross-validation to evaluate the accuracy of classification. For each task, the total samples are randomly partitioned into 5 equal-sized subsets. Among the 5 subsets, four subsets are used as the training set while the remaining one is used as testing set. This process is then repeated 5 times, and each of the 5 subsets is used exactly once as the testing set.

V. RESULTS

A. The robustness of FSR module

Fig. 6 shows the result of the response of FSR at different pressure and contact area. The pressing phase and the releasing phase are displayed separately. For the same subarea, the response of FSR shows high consistency both in the pressing phase and releasing phase. While for different contact area, when the force acted on the finger is identical, the average conductance of FSR is different but the trend is similar. This behaviour is consistent with our analysis in section II. It can be seen from Fig. 6 that the break-out force (due to the structure of FSR, external force smaller than this value will not cause the changing in resistance value) of FSR in our sensor still exists (about 1-2N). During practice applications, this can be overcome by applying a pre-load to the FSR. Furthermore, when the external force is small (about 0-5N),

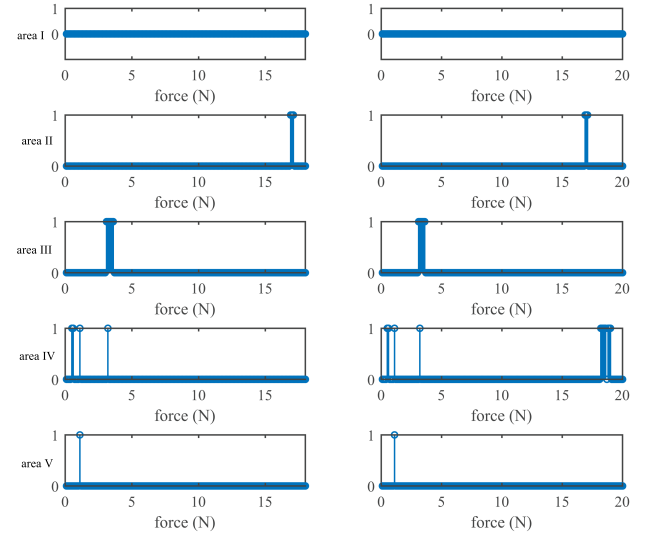


Fig. 7. The result of K-S test of the response of FSR under different external force (0.1N to 20N, with a step size of 0.1N) and different test. The result equals to 1 means that the test rejects the null hypothesis (H_0) at the significance level of 5%, while the result equals to 0 means that the test fails to reject the null hypothesis at the 5% significance level.

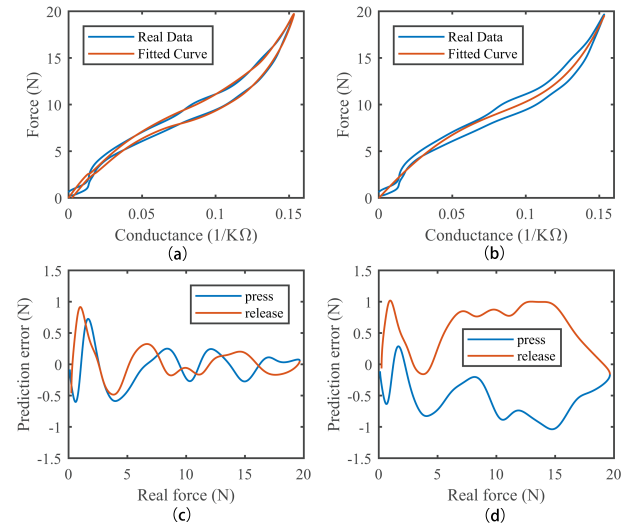


Fig. 8. The results of calibrating the FSR for contact force measurement. (a) The fitted curve of FSR considering the hysteresis (the calibration function is (3)). (b) The fitted curve of FSR neglecting the hysteresis (the calibration function is a fourth-order polynomial equation without the term of I_t in (3)). (c) The absolute prediction error of force in (a) during pressing and releasing stages. (d) The absolute prediction error of force in (b) during pressing and releasing stages.

the influence of contact point location on FSR is very small, and this phenomenon agrees with our analysis in section II. As the external force increases, the influence of contact point location on the response of FSR emerges.

Fig. 7 shows the result of the normal distribution test of the response of FSR at each sample force (0.1N to 20N, with a step size of 0.1N) across different tests for different subarea. The test result equals to 1 means that the K-S test rejects the null hypothesis (H_0) at the significance level of 5%. In other words, this means that we have to accept the conclusion that the different samples come from a normal distribution. While the result equals to 0 means that the K-S test fails to reject the null hypothesis (which means we have to accept H_1) at the 5% significance level. It can be seen from Fig. 7 that under different external forces, for the same subarea, almost all the test results are equal to 1, which means that the FSR shows a high consistency during both the pressing phase and the releasing phase. This is also in agreement with the results shown in Fig. 6, because it can be seen in Fig. 6 that the standard error for each curve is very small relative to the mean value.

B. Calibration of FSR

Fig. 8 shows the results of two approaches to calibrate the FSR for contact force measurement, that is, considering and neglecting the hysteresis of FSR. It is obvious in Fig. 8(a) that the hysteresis of FSR is non-negligible, since the measured force-conductance curve during pressing and releasing have significant difference. Fig. 8(a) shows the fitted curve that uses the calibration function in (3). As it is shown, the fitted curve matches the measured data very well, and the hysteresis characteristic of measured data also appears in the fitted curve. Fig. 8(c) shows the result of force prediction error that uses the calibration method in Fig. 8(a). The absolute prediction error is less than 0.5N when the force is larger than 5N. However, because of the influence of the dead zone (under break force), the prediction error in small force is still significant. By contrast, Fig. 8(b) shows the fitted curve neglecting the moving integral term in (3). In this way, the error due to the hysteresis is significant during both the pressing stage and releasing stage. As shown in Fig. 8(d), the force prediction error that uses the calibration method in Fig. 8(b) is relative larger than that in Fig. 8(c). According to our calculations, the average force prediction error above the breaking force for five subarea is about 7.34%.

C. Contact point location

Fig. 9 shows the typical waveforms of the normalized PVDF signal for five subareas at experiment I. It can be seen from Fig. 9 that for different subarea, the waveform of PVDF has an intuitive difference, while for the same subarea, the waveform shows a consistent response during different tests. This result agrees with the analysis in section II, and it shows a great potential for a higher resolution of contact point location. We also noticed that the waveforms in Fig. 9 (d) and Fig. 9(e) are similar, but still have difference in some details. This is also in agreement with the theoretical analysis, since the positions

of subarea IV and subarea V are symmetrically. However, the shape of PVDF is not symmetrically at subarea IV and subarea V, because it has a circular truncated cone shape. Thus, due to the high sensitivity and robustness of PVDF, the PVDF signals at subarea IV and subarea V are still easy to distinguish.

Fig. 10 gives a complete result of the discrimination of contact point in both conditions (precise loading that controlled by the micro-controller and roughly loading that controlled by the operator). As shown in Fig. 10(a), for five precise contact position, the average accuracy for the combination of different feature and different classifier is relatively high. For several conditions, the accuracy values are 100%. When using the Wavelet Packet Decomposition method for feature extraction, the accuracy of all the classifier is above 96%, which means the influence of classifier is small. In other words, the data or the features of data is robust. This is consistent with the intuition from Fig. 9, in which the information of low frequency band (less than 1Hz) of PVDF signal at different contact area is different from each other. Fig. 10(b) shows another condition that the load is performed by the operator, which can be regarded as five contact areas. The maximum average accuracy reaches 94.8% when using the Freq. Comp. as the feature extraction method and the Gaussian kernel SVM as the classifier. Except for several conditions, all the accuracy values are close to 90%. Compared to the result in (a), the accuracy dropped a little in this case. This is because the contact positions in (a) are stable in each area, however, when loaded by the operator, the contact position and the maximum force are both fluctuant.

D. Texture recognition

Fig. 11(a) shows the accuracy of the combination of each feature and classifier for texture recognition. As shown in Fig. 11(a), for five natural surfaces, the maximum accuracy is $94.1\% \pm 0.7\%$ with the db2 ($n=6$) feature and Gaussian kernel SVM classifier. When using the Wavelet Packet Decomposition (WPD) method for feature extraction, for both k NN and SVM classifiers, the average accuracy is close to 90%, and the WPD method for feature extraction is proved to be the most efficient method for feature extraction in this work.

Fig. 11(b) shows the confusion matrix of one experiment that uses the db2 ($n=6$) as features and Gaussian kernel SVM as the classifier. The classification accuracy of texture 1 (table surface, hard, rough), texture 2 (frosted plastic sheet, hard, medium rough), and texture 3 (acrylic sheet, hard, smooth) are relatively lower than texture 4 (flannelette) and texture 5 (Cotton).

VI. DISCUSSION

From the above results, we confirmed that our designed fingertip tactile sensor has a good comprehensive performance in contact force measuring, contact point location and texture recognition. This makes it very suitable for prosthetic hand applications. Although the model used for the calibration of FSR is simple, the result is acceptable for prosthesis applications. The average relative error for force measuring is about 7.34% above the dead zone of FSR. This accuracy

TABLE II
PERFORMANCE OF THE FINGERTIP SENSOR

| CHARACTERISTICS | VALUE |
|---|-------------------------------------|
| Transduction method | Piezoelectric & piezoresistive |
| Fabrication technology | 3D printing & PDMS casting |
| Number of sensing element | Two (one FSR & one PVDF) |
| Distinguishable area | ≥ 5 |
| Spacial resolution | $\sim 6\text{mm} \times 5\text{mm}$ |
| Accuracy of classify distinguishable area | $\geq 96\%$ |
| Average force precision error | 7.34% (five subareas) |
| Force range | Up to 100N (according to FSR guide) |

is close to the results of some complicated array sensors (e.g. in [16], the average relative error of the fingertip three-axis sensor in z -axes is 3.5%. In [18], the average relative error of the piezoelectric tactile sensor array is 10.68% with a standard deviation of 6.84%). Table II gives a simple summary about the performance of our proposed sensors.

Contact point location during grasp manipulation is an important function for the tactile sensor both in the sensory feedback to users and the feedback to the prosthesis itself. Traditionally, contact point location can only be achieved by array sensors, while the fabrication of an array sensor highly depends on the specialized equipment, such as the MEMS device, electrospinning device, screen printing and laser structuring device, and so on. Furthermore, for an array sensor, the processing circuit is also complicated, and many processing units are needed to exclude the electromagnetic noise due to the high sensitivity of each sensor element. For these reasons, the cost of an array sensor is extremely high, which limits its application in the prosthesis. In this work, we put forward a novel concept and method to discriminate the contact point with only one sensor element. The concept is based on the nonuniform deformation of the elastic material PDMS and the high sensitivity of the PVDF. Experimental results show that with commonly used pattern recognition methods, the accuracy of discriminating five contact subareas is not less than 96% while using the WPD method for feature extraction. With this concept, the spatial resolution of contact point discrimination can also be improved in the future. In order to increase the spatial resolution, we need to enlarge the difference of the output of PVDF when the force acts on different areas. This may need more profound research on

the shape of PVDF (e.g. in [39], the PVDF film is shaped into semi-circular to improve the resolution of the airborne transducer).

In this work, we divided the sensitive area of the finger into five subareas. Although this spatial resolution is relatively lower than those commercial array sensors, it is still able to meet the requirement of prosthetic hand application. According to the dimension (envelop size: 15mm x 18mm, as shown in Fig. 2(a)) of the sensitive area of our sensor, this spatial resolution is about 5mm, which is comparable to the works by other researchers (e.g. in [7], [40], the spatial resolution is about 5.5mm). What's more, according to the research about the deformation of the human fingertip at contact [41], the contact area of the fingertip is about 60mm^2 when the indentation is 2mm, while the corresponding force is about 0.5N. This means that for most grasp tasks of the human hand, the contact area between the fingertip and the object is more than 60mm^2 (since the contact area increases with the contact force, and for most grasp tasks in daily living, the grasp force will be larger than 0.5N). In our design, the average area for the five subareas is about 50mm^2 . This also indicates that our design is reasonable. Finally, we tested the ability of texture recognition of our sensor. For five common textures in daily life, the best result shows that the accuracy is $94.1\%\pm 0.7\%$, which is an excellent performance even compared to other studies that use more complex designs [27].

Generally speaking, we proposed a novel fingertip sensor with the FSR and PVDF for force measuring, contact point location, and texture recognition in this paper. The PVDF is a kind of material that is commonly used in tactile sensors for texture recognition in high-frequency response. In this

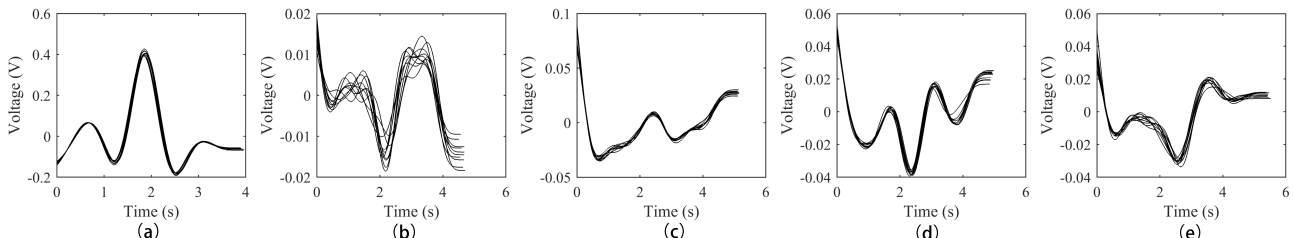


Fig. 9. Example data of PVDF signal in experiment I. The original signal is filtered by a 6th-order lowpass digital Butterworth filter with cutoff frequency 1Hz. (a) to (e) corresponds to subarea I to subarea V.

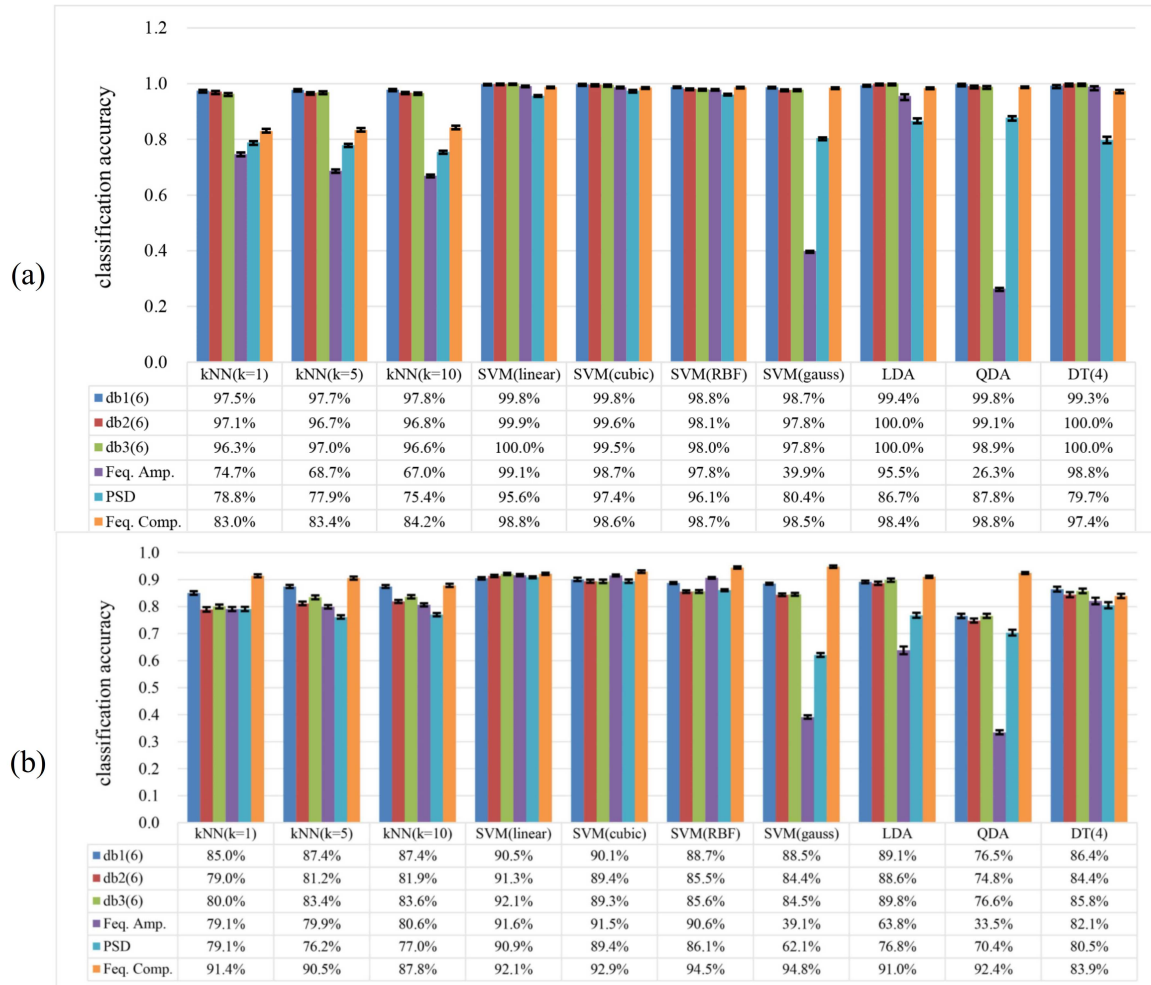


Fig. 10. Classification accuracy of each classifier and feature for contact point location.(a) The sensor was loaded by the device. (b) The sensor was loaded by hand of the operator.

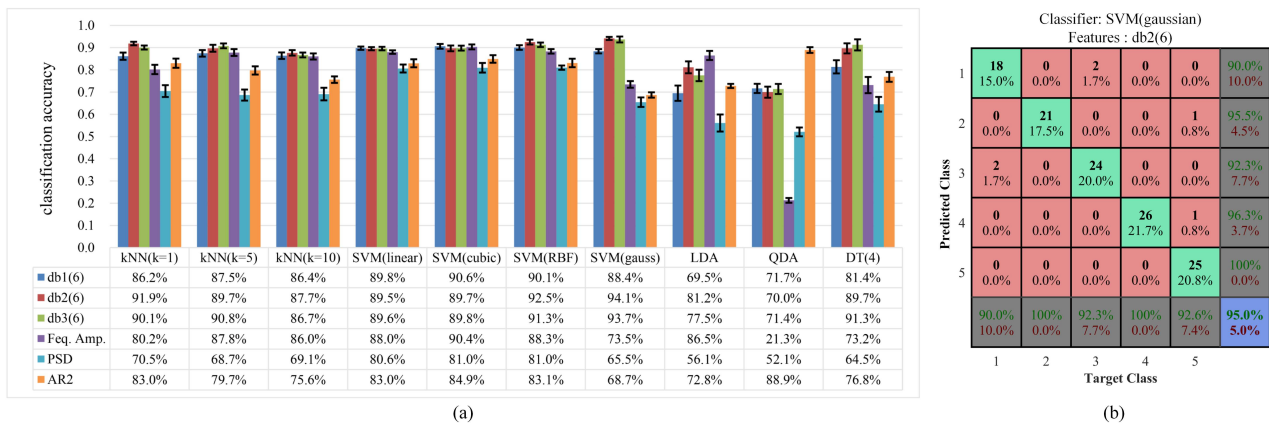


Fig. 11. (a) Classification accuracy of each classifier and feature for texture recognition. (b) Confusion matrix of one experiment that use the db2(6) as features and the Gaussian kernel SVM as classifier.

work, we use the high-frequency response of PVDF for texture recognition and the low-frequency response of PVDF for contact point location. The main idea is that different contact point will cause different deformation to the shape of PVDF, and due to the high sensitivity of PVDF, the tiny difference during deformation will result in different electrical response. The experimental results show that this method is feasible. It should be noted that we only used one sensing element for both texture recognition and contact point location. This method has the potential to be widely applied, especially for those applications in which the space and cost are critically limited. Although the proposed method has been proved effective by experiments, there are still many details that need to be further studied. If we can theoretically model the relationship between the response to the contact point and the shape of PVDF, and then optimize the shape the PVDF through the model, the performance of the sensor might be better.

VII. CONCLUSION

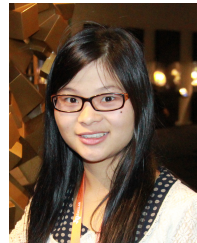
In this work, we proposed a novel design concept of a fingertip tactile sensor. The concept uses only one sensor element to estimate the location of the contact point in the finger bed. The detailed structures, fabrication, and working principle of the sensor are introduced in this paper. Comprehensive experiments from three aspects were conducted to evaluate the performance of the sensor. Experimental results showed that the sensor has an overall good performance in force measuring, contact point estimation, and texture recognition. The dimension and appearance of our fingertip are similar to the human finger. The simplified structure design makes it convenient to be integrated into a prosthetic hand.

There are also possible future works we could carry out. First, we would like to further study the shape of PVDF to improve the spatial resolution of contact point estimation. Second, the shear force is important for grasping and the shear force is frequently induced during the contact. Therefore, the measuring of shear force and its influence on the repeatability of the FSR sensor and the PVDF sensor output could also be further studied.

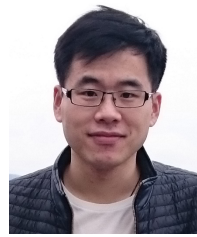
REFERENCES

- [1] L. Osborn, R. R. Kaliki, A. B. Soares, and N. V. Thakor, "Neuromimetic event-based detection for closed-loop tactile feedback control of upper limb prostheses," *IEEE Trans. Haptics*, vol. 9, no. 2, pp. 196–206, 2016.
- [2] Z. Kappassov, J.-A. Corrales, and V. Perdereau, "Tactile sensing in dexterous robot hands - review," *Rob. Auton. Syst.*, vol. 74, pp. 195–220, 2015.
- [3] L. Zou, C. Ge, Z. J. Wang, E. Cretu, and X. Li, "Novel tactile sensor technology and smart tactile sensing systems: A review," *Sensors*, vol. 17, no. 11, p. 2653, 2017.
- [4] (2018,Jun.) i-limb quantum, touch bionics. [Online]. Available: <http://www.touchbionics.com/products/active-prostheses/i-limb-quantum>
- [5] (2018,Jun.) bebionic hand, ottobock Inc. [Online]. Available: <https://www.ottobockus.com/prosthetics/upper-limb-prosthetics/solution-overview/bebionic-hand/>
- [6] (2018,Jun.) Vincent systems gmbh. [Online]. Available: <https://vincentsystems.de/en/>
- [7] R. Koiva, M. Zenker, C. Schürmann, R. Haschke, and H. J. Ritter, "A highly sensitive 3d-shaped tactile sensor," in *Advanced Intelligent Mechatronics (AIM), 2013 IEEE/ASME International Conference on*. IEEE, 2013, pp. 1084–1089.
- [8] C.-H. Chuang, M.-S. Wang, Y.-C. Yu, C.-L. Mu, K.-F. Lu, and C.-T. Lin, "Flexible tactile sensor for the grasping control of robot fingers," in *Advanced Robotics and Intelligent Systems (ARIS), 2013 International Conference on*. IEEE, 2013, pp. 141–146.
- [9] T. Zhang, H. Liu, L. Jiang, S. Fan, and J. Yang, "Development of a flexible 3-d tactile sensor system for anthropomorphic artificial hand," *IEEE Sensors J.*, vol. 13, no. 2, pp. 510–518, 2013.
- [10] A. Massaro, F. Spano, A. Lay-Ekuakille, P. Cazzato, R. Cingolani, and A. Athanassiou, "Design and characterization of a nanocomposite pressure sensor implemented in a tactile robotic system," *IEEE Transactions on Instrumentation and Measurement*, vol. 60, no. 8, pp. 2967–2975, Aug 2011.
- [11] L. Min, L. Shan, T. Nanayakkara, L. D. Seneviratne, P. Dasgupta, and K. Althoefer, "Multi-fingered haptic palpation using pneumatic feedback actuators," *Sensors & Actuators A Physical*, vol. 218, no. 10, pp. 132–141, 2014.
- [12] C. Shi, T. Li, and H. Ren, "A millinewton resolution fiber bragg grating-based catheter two-dimensional distal force sensor for cardiac catheterization," *IEEE Sensors Journal*, vol. 18, no. 4, pp. 1539–1546, Feb 2018.
- [13] T. Li, C. Shi, and H. Ren, "A high-sensitivity tactile sensor array based on fiber bragg grating sensing for tissue palpation in minimally invasive surgery," *IEEE/ASME Transactions on Mechatronics*, vol. 23, no. 5, pp. 2306–2315, Oct 2018.
- [14] F. Vecchi, C. Freschi, S. Micera, A. M. Sabatini, P. Dario, R. Sacchetti *et al.*, "Experimental evaluation of two commercial force sensors for applications in biomechanics and motor control," in *5th Ann. Conf. of Int. FES*, 2000.
- [15] W. Fukui, F. Kobayashi, F. Kojima, H. Nakamoto, N. Immura, T. Maeda, and H. Shirasawa, "High-speed tactile sensing for array-type tactile sensor and object manipulation based on tactile information," *J. Robotics*, vol. 2011, 2011.
- [16] T. Zhang, L. Jiang, X. Wu, W. Feng, D. Zhou, and H. Liu, "Fingertip three-axis tactile sensor for multifingered grasping," *IEEE/ASME Trans. Mechatron.*, vol. 20, no. 4, pp. 1875–1885, 2015.
- [17] A. Schmitz, M. Maggiali, L. Natale, B. Bonino, and G. Metta, "A tactile sensor for the fingertips of the humanoid robot icub," in *Intelligent Robots and Systems (IROS), 2010 IEEE/RSJ International Conference on*. IEEE, 2010, pp. 2212–2217.
- [18] P. Yu, W. Liu, C. Gu, X. Cheng, and X. Fu, "Flexible piezoelectric tactile sensor array for dynamic three-axis force measurement," *Sensors*, vol. 16, no. 6, p. 819, 2016.
- [19] C. M. Oddo, L. Beccai, M. Felder, F. Giovacchini, and M. C. Carrozza, "Artificial roughness encoding with a bio-inspired mems-based tactile sensor array," *Sensors*, vol. 9, no. 5, pp. 3161–3183, 2009.
- [20] S. Emamian, B. B. Narakathu, A. A. Chlaihawi, B. J. Bazuin, and M. Z. Atashbar, "Screen printing of flexible piezoelectric based device on polyethylene terephthalate (pet) and paper for touch and force sensing applications," *Sens. Actuators A Phys.*, vol. 263, pp. 639–647, 2017.
- [21] A. Schmitz, M. Maggiali, M. Randazzo, L. Natale, and G. Metta, "A prototype fingertip with high spatial resolution pressure sensing for the robot icub," in *Humanoid Robots, 2008. Humanoids 2008. 8th IEEE-RAS International Conference on*. IEEE, 2008, pp. 423–428.
- [22] (2018,Jun.) Pressure mapping sensors,tekscan Inc. [Online]. Available: <https://www.tekscan.com/pressure-mapping-sensors>
- [23] (2018,Jun.) Fingertips pressure sensor system, pps Inc. [Online]. Available: <https://pressureprofile.com/fingertips>
- [24] (2018,Jun.) Wts-ft weiss robotics gmbh & co. [Online]. Available: <https://www.weiss-robotics.com/en/produkte/unkategorisiert/wts-ft-en/>
- [25] (2018,Jun.) Syntouch announces the biotac sp, syntouch syntouch, Inc. [Online]. Available: <https://www.syntouchinc.com/en/syntouch-announces-the-biotac-sp/>
- [26] X. Wang, F. Sun, G. Yin, Y. Wang, B. Liu, and M. Dong, "Tactile-sensing based on flexible pvdf nanofibers via electrospinning: A review," *Sensors*, vol. 18, no. 2, p. 330, 2018.
- [27] H. Hu, Y. Han, A. Song, S. Chen, C. Wang, and Z. Wang, "A finger-shaped tactile sensor for fabric surfaces evaluation by 2-dimensional active sliding touch," *Sensors*, vol. 14, no. 3, pp. 4899–4913, 2014.
- [28] H. Khan, A. Razmjou, W. M. Ebrahimi, A. Kottapalli, and M. Asadnia, "Sensitive and flexible polymeric strain sensor for accurate human motion monitoring," *Sensors*, vol. 18, no. 2, p. 418, 2018.
- [29] A. Ghasemi and S. Zahediasl, "Normality tests for statistical analysis: a guide for non-statisticians," *Int. J. Endocrinol. Metab.*, vol. 10, no. 2, p. 486, 2012.
- [30] M. Kalantari, M. Ramezanifard, R. Ahmadi, J. Dargahi, and J. Kovcse, "Design, fabrication, and testing of a piezoresistive hardness sensor in

- minimally invasive surgery,” in *Haptics Symposium, 2010 IEEE*. IEEE, 2010, pp. 431–437.
- [31] N. K. Rana, “Application of force sensing resistor (fsr) in design of pressure scanning system for plantar pressure measurement,” in *Second International Conference on Computer & Electrical Engineering*, 2009.
- [32] C. Lebosse, B. Bayle, M. de Mathelin, and P. Renaud, “Nonlinear modeling of low cost force sensors,” in *Robotics and Automation, 2008. ICRA 2008. IEEE International Conference on*. IEEE, 2008, pp. 3437–3442.
- [33] L. Paredes-Madrid, A. Matute, A. F. Cruz-Pacheco, C. A. Parra-Vargas, and E. I. Gutiérrez-Velásquez, “Experimental characterization, modeling and compensation of hysteresis in force sensing resistors,” *Dyna*, vol. 85, no. 205, pp. 191–198, 2018.
- [34] L. Paredes-Madrid, C. A. Palacio, A. Matute, and C. A. P. Vargas, “Underlying physics of conductive polymer composites and force sensing resistors (fsrs) under static loading conditions,” *Sensors*, vol. 17, no. 9, p. 1334, 2017.
- [35] A. S. Sadun, J. Jalani, and J. A. Sukor, “Force sensing resistor (fsr): a brief overview and the low-cost sensor for active compliance control,” in *International Workshop on Pattern Recognition*, 2016.
- [36] R. S. Hall, G. T. Desmoulin, and T. E. Milner, “A technique for conditioning and calibrating force-sensing resistors for repeatable and reliable measurement of compressive force,” *Journal of Biomechanics*, vol. 41, no. 16, pp. 3492–3495, 2008.
- [37] I. Daubechies, “Ten lectures on wavelets,” *Computers in Physics*, vol. 6, no. 3, pp. 1671–1671, 1998.
- [38] W. Press, S. Teukolsky, W. Vetterline, and B. P. Flannery, “Numerical recipes: The art of scientific computing, ch. 12-13,” 2007.
- [39] K. Gürkan and A. Akan, “Simulation and measurement of air-coupled semi-circular and conical pdvf sensors,” *IEEE Sensors J.*, vol. 16, no. 4, pp. 983–988, 2016.
- [40] P. Cerveri, M. Quinzi, D. Bovio, and C. A. Frigo, “A novel wearable apparatus to measure fingertip forces in manipulation tasks based on mems barometric sensors,” *IEEE Trans. Haptics*, vol. 10, no. 3, pp. 317–324, 2017.
- [41] M. L. D’Angelo, F. Cannella, M. Bianchi, M. D’Imperio, E. Battaglia, M. Poggiani, G. Rossi, A. Bicchi, and D. G. Caldwell, “An integrated approach to characterize the behavior of a human fingertip in contact with a silica window,” *IEEE Trans. Haptics*, vol. 10, no. 1, pp. 123–129, 2017.



Luyao Chen received the B.S. degree in Electronic Science and Technology from Huazhong Normal University, Wuhan, China, in 2012. She is currently pursuing the Ph.D. degree in the Microelectronics and Solid-state Electronics from Huazhong University of Science and Technology, Wuhan, China. Her research interests include neural electrodes, neural recording systems, and neural modulations through electrical and ultrasound stimulations.



Zhaolong Gao received the B.S. degree in control science and engineering from Huazhong University of Science and Technology, Wuhan, China, in 2011. He is currently pursuing the Ph.D. degree in the control science and engineering from the Huazhong University of Science and Technology, Wuhan, China. His research interests include robotics, haptics and tactile feedback of prosthesis.



Jiuqi Han received his B.E. degree from Beijing University of Chemical Technology, Beijing, China, in 2010, the M.E. degree from University of Chinese Academy of Sciences in Beijing, China, in 2013, and the Ph.D. degree from the Institute of Automation, Chinese Academy of Sciences, Beijing, China in 2016. His research interests include pattern recognition, brain-machine interface and robotics, etc.



Ang Ke received the B.S. degree in mechanical science and engineering from Huazhong University of Science and Technology, Wuhan, China, in 2014. He is currently pursuing the Ph.D. degree in the control science and engineering from the Huazhong University of Science and Technology, Wuhan, China. His research interests include upper limb prosthesis, rehabilitation, robotics, and brain-machine interface.



Changyong Wang received his doctorate degree in School of Stomatology, Fourth Military Medical University in 1998. Now, he is director of Tissue Engineering Research Center, Academy of Military Medical Sciences, director of branch of Bio-material of CSMS, vice chairman of the Chinese Society of Bio-manufacturing Engineering, expert of Strategy Study of National Manned Space Development of General Armament Department, and advanced research of space medical sciences. His research interests lie in biomaterial, tissue engineering, neural engineering, and brain-machine interface.



Jian Huang (M’07-SM’17) graduated from Huazhong University of Science and Technology (HUST), Wuhan, China, in 1997 and received the Master of Engineering degree and the Ph.D. degree from HUST in 2000 and 2005, respectively. From 2006 to 2008, he was a Postdoctoral Researcher at the Department of MicroNano System Engineering and the Department of Mechano-Informatics and Systems, Nagoya University, Japan. He is currently a Full Professor with the School of Artificial Intelligence and Automation, HUST. His main research interests include rehabilitation robot, robotic assembly, networked control systems and bioinformatics. He is serving as the Associate Editor of IEEE Transactions on Fuzzy Systems.



Jin Zhou received her Ph.D. degree in Institute of Basic Medical Sciences, Academy of Military Medical Sciences in 2010. She is one of the academic leaders in the field of establishing an intelligent control platform based on brain-computer interface technology in the Military Medical Research Institute. Her research interests include tissue engineering, neural engineering, and brain-machine interface.



Jiping He (S'86-M'89-SM'97) received the B.S. degree in control engineering from the Huazhong University of Science and Technology, Wuhan, China, in 1982, and the M.S. and Ph.D. degrees in electrical engineering from the University of Maryland, College Park, MD, USA, in 1984 and 1988, respectively. He joined Arizona State University, Tempe, AZ, USA, as an Associate Professor in 1994 where is now a Professor of bioengineering. Director of the Center for Neural Interfaces Design. His research interests include implantable neural interface technology, cortical and spinal cord recording and stimulation for sensorimotor adaptation, application of robotics and virtual reality research to neuromotor rehabilitation, and prosthetic devices.